# The effect of water on the post-spinel transition and evidence for extreme water contents at the bottom of the transition zone

Joshua M. R. Muir[1], Feiwu Zhang[1] and John P. Brodholt[2]

1) Institute of Geochemistry, Chinese Academy of Sciences, 99 West Lincheng Road, Guiyang, Guizhou 550081, China
2) Department of Earth Sciences, University College London, London, WC1E 6BT, UK

j.m.r.muir@mail.gyig.ac.cn

Word count: 5559

Abstract:

The transition of ringwoodite to bridgmanite and periclase (the post-spinel transition) is a strong control on the 660 phase discontinuity and the boundary between the transition zone and the lower mantle. The transition zone may contain significant amounts of water and thus the effect of water on the post-spinel transition must be known to correctly determine its properties. In this paper we examine the transition of ringwoodite to bridgmanite and periclase in both dry and wet conditions using density functional theory (DFT). In the dry case we calculate a high negative Clapeyron slope (-3.19±0.19 MPa/K at 1873 K). We also find that the Clapeyron slope is significantly nonlinear with temperature and much lower at 1000 K (-1.31 MPa/K) or if determined by linear interpolation from 1000 K (-2.37 MPa/K). The addition of water causes a large broadening of the transition through the development of a phase loop. Seismic studies suggest that the 660 km discontinuity is narrower than 2 km. For this to be the case our results suggest that the water content at the bottom of the transition zone needs to be either less than ~700 ppm or, alternatively, above ~8000 ppm (assuming an effective transition width near the maximum transition width). In the latter case this is above the saturation limit for bridgmanite and so will be accompanied by the production of a free water phase/hydrous melt. The hydration of ringwoodite also causes the onset of the transition to deepen with 1 wt% water increasing the depth of the transition by about 8 km. This is relatively small compared to seismically observed variations in the

660 km discontinuity of around 35 km and so water alone cannot account for the observed 660 km discontinuity topography. Water causes no substantial changes to the Clapeyron slope of the transition, so the 660 km topography could be explained by thermal variations of ~500 K.

Keywords: Ringwoodite, Bridgmanite, Water, 660 discontinuity, Post-spinel transition, DFT

## 1. Introduction:

The transformation of ringwoodite to bridgmanite and MgO is an important reaction and is generally considered to be responsible for the seismic discontinuity that occurs at an average depth of 647-654 km (Gu and Dziewonski, 2002) - the so-called 660 km discontinuity. This discontinuity defines the boundary between the transition zone and the lower mantle, and an understanding of the nature of this transition is critical for understanding processes between the upper mantle and transition zone and the lower mantle.

There have been a number of experimental and theoretical studies on this transition, but the Clapeyron slope still remains quite uncertain. Experiments in literature have produced two quite different ranges of this slope - one with relatively low slopes ranging from -0.2-1.3 MPa/K (Fei et al., 2004; Ghosh et al., 2013; Hernandez et al., 2013; Ishii et al., 2011; Katsura et al., 2003; Kojitani et al., 2016; Litasov et al., 2005a) and one with higher slopes ranging from -2.6-3.6 MPa/K (Akaogi et al., 2007; Bina and Helffrich, 1994; Hernandez et al., 2015; Irifune et al., 1998; Shim et al., 2001; Yu et al., 2007), although some intermediate values up to 2 MPa/K are also observed (Ishii et al., 2011; Katsura et al., 2003). The exact cause of this discrepancy is still unclear, however, obtaining the correct value for the Clapeyron slope is highly important for interpreting the topography of the 660 km in terms of temperature and composition.

One important compositional parameter is hydration. Since the transition zone can potentially contain up to ~2 wt% water, observed variations in the depth of the 660 km discontinuity could be used to map out the water content of the transition zone (e.g. Houser (2016), Wang et al. (2020)). A series of studies have shown that water can shift the phase transition to higher pressures (from about ~0.2 to

1.3 GPa depending on the amount of water and the particular study) (Ghosh et al., 2013; Higo et al., 2001; Litasov et al., 2005b), while at the same time water may also increase the Clapeyron slope. For instance, Ghosh et al (2012) suggests that the Clapeyron slope increases from -0.4-0.7 MPa/K in the dry case to -3.1-3.2 MPa/K with 2 wt% water (Ghosh et al., 2013). Such a large effect would mean that wet regions of the transition zone would have depressed phase transitions which should be seismically visible. However, as with measuring even the nominally dry slope of the ringwoodite phase transition, there is considerable uncertainty over the effect of water on the depth and slope of the post-spinel transition.

In this work we use Density-Functional Theory (DFT) to examine the post-spinel transition and the effect of water at high temperatures and pressures. We calculate the depth of the transition, its slope, and the width of the transition as a function of temperature and water content.

## 2. Methods:

### *2.1 Calculation Details*

We used DFT to calculate the free energies of $Mg_2SiO_4$ ringwoodite and $MgSiO_3$ bridgmanite as a function of temperature, pressure and water concentration. We assumed that periclase is essentially dry as shown previously (Muir and Brodholt, 2018) and so only dry calculations were performed on that phase. Free energy calculations were carried out at 20, 25 and 30 GPa at 0, 1000, 1500 and 2000 K with further athermal (0 K) calculations carried out at 15, 17.5, 22.5, 27.5, 32.5 and 35 GPa. Once these free energies were determined phase diagrams were constructed by fitting polynomials to the free energies as a function of P, T and composition. The energy of each phase was then determined by mixing the dry and hydrous proportions of each phase as outlined below. To find the 3-phase loop we fitted the common tangent to $2^{nd}$-order polynomial curves of free energy vs water concentration for ringwoodite and bridgmanite+periclase phases. The derivatives of these free energy curves are very similar for the two phases and so the error in the common tangent is quite large as discussed later in the text.

All simulations were carried out with the DFT code VASP (Kresse and Furthmuller, 1996) using the projector-augmented-wave (PAW) method (Kresse and Joubert, 1999) and the PBE

85 formulation of GGA (Perdew et al., 2008). For Mg atoms the semicore 2p states were treated as valence.
86 All runs were spin-polarised.
87 Static calculations were run with an energy cutoff of 600 eV, 6x6x6 k points and self-consistent
88 runs that were relaxed to within $10^{-8}$ eV. Molecular dynamics (MD) simulations were run to obtain
89 properties at high T using an NVT ensemble with the Nosé thermostat (Nose, 1984) and with Nosé
90 frequencies of ~20 THz. MD calculations were run at the gamma point with a cutoff of 600 eV,
91 relaxation to within $10^{-4}$ eV, and properties were averaged over at least 10 ps (though all properties
92 were fully converged by 6 ps). For calculating the force constant matrix, phonons were calculated using
93 the finite difference method with at least 5 different volumes for every system and processing was done
94 with the Phonopy code (Togo, 2015). For force constant matrix calculations it was necessary to increase
95 the energy cutoff to 1000 eV to get sufficient accuracy in the phonons. Increasing the energy cutoff
96 further to 1500 eV changed the energy of dry ringwoodite and bridgmanite (under a QHA approach) by
97 <0.003 meV/atom at 2000 K and 25 GPa. Changing the cutoff changes the Pulay stress but this effect
98 is extremely small. By running the relaxed structure determined at 600 eV with a cutoff at 1000 eV we
99 find the energy change from a structure relaxed at 1000 eV is <0.005 meV/atom. When calculating
100 phonons only the gamma point was used as this is the only physical meaningful point when using the
101 finite difference method. While this will introduce some additional error in the calculation, as we are
102 calculating free energy differences the errors induced from only having a single q-point will largely
103 cancel out. The effect of vibrational entropy is also very small as discussed below so this is not a
104 significant source of error.
105 $MgSiO_3$ was simulated with an 80 atom unit cell, MgO with a 64 atom unit cell and $Mg_2SiO_4$ a
106 56 atom unit cell. To determine the energy of wet systems we assume most of the water is incorporated
107 as substituted for Mg (Hernandez et al., 2013; Muir and Brodholt, 2018) and so energies were
108 determined with 1 Mg vacancy that was filled with 2 hydrogen atoms. This is a concentration of 1.1
109 wt% water in the bridgmanite and 1.6 wt% in the ringwoodite. To check the effect of water
110 concentration we calculated the enthalpy difference of the wet post-spinel reaction (reaction 2 in the
111 text) as a function of water concentration between 0.14 wt% and 12 wt% with the results shown in
112 Figure S1. While there is a clear trend in the reaction energy with increasing water concentration, this

trend is very small (<1 meV/atom) and smaller than the errors induced by DFT approximations (typically on the order of a few meV/atom) which means that it is negligible in our free energy calculations. Thus we treat the wet reaction and the dry reaction as ideal mixtures in Reaction 1 and Reaction 2 to create Reaction 3:

$Mg_2SiO_4 \rightarrow MgSiO_3 + MgO$ Reaction 1

$(2H)MgSiO_4 \rightarrow (2H)SiO_3 + MgO$ Reaction 2

$Mg_{2-x}(2H)_xSiO_4 \rightarrow Mg_{1-x}(2H)_xSiO_3 + MgO$ Reaction 3

where Reaction 2 is Reaction 3 with x=1.

*2.2 Free energy:*

To determine the entropic part of the free energy we use the quasi-harmonic approximation (QHA). While this has previously been used for the dry post-spinel reaction (Hernandez et al., 2013; Hernandez et al., 2015; Yu et al., 2007) it is questionable whether this holds for the wet phase transition because of the high mobility of the hydrogen in the Mg vacancy (see Figure S2). To test whether the QHA approximation works for the hydrogen bearing systems we tried three other methods:

1) Using just the enthalpy determined from a normal molecular dynamics run (which includes thermal expansion to the correct cell size) (ENTH)
2) Adding in an additional entropy term to the enthalpy determined via integrating the vibrational density of states (VDOS), which is the Fourier transform of the Velocity Autocorrelation function (MD)
3) A thermodynamic integration from the QHA to the molecular dynamics run (the method for this is described in the supplementary methods) (TI).

As shown in Table 1 all of these methods produce similar answers and in particular the MD, QHA and TI methods are nearly identical. This is because while the hydrated system has significant anharmonicity due to the movement of the hydrogens, the anharmonicity is very similar for all hydrated systems and thus cancels out when calculating free energy differences. We shall, therefore, present results from the QHA analysis from here on.

Another feature that needs to be addressed is the configurational entropy difference between wet bridgmanite and wet ringwoodite. This has two parts: 1) the configuration of hydrogens in the

vacancy and 2) the configuration of vacancies in the unit cell. The first case is complicated by the fact that hydrogens do not remain confined to a single site at high temperature in either ringwoodite (Figure S2) or bridgmanite (Muir and Brodholt, 2018). This is discussed in more detail in the supplementary information but in short we assumed all arrangements of hydrogen were equivalent in both ringwoodite and bridgmanite and calculated their entropy with the Boltzmann entropy formula. In the second case we assumed all vacancy arrangements were equivalent and that there is no long range order to wet vacancies. We then used the Boltzmann entropy formula with the Stirling approximation to calculate the configurational entropy of both the hydrogen and the water induced vacancies in each system.

*2.3 Pressure Correction*

While DFT generally reliably reproduces pressure derivatives, the absolute pressures reported by DFT are known to be systematically incorrect such that they are shifted in one direction. This arises due to the fact that different approximations of the exchange correlation give different pressures shifts, with GGA methods (such as the PBE approximation used here) overestimating volume and pressure and LDA methods doing the reverse, although to a lesser extent. This GGA error was accounted for by the following equations:

$$P(V,T) = \frac{K_0^{exp}}{K_0^{DFT}} P^{DFT}\left(V\frac{V_0^{DFT}}{V_0^{exp}}\right) + \Delta P^{DFT}(V,T) \quad \text{Equation 1}$$

$$F(V,T) = F\left(V_0^{exp}\right) + \frac{V_0^{exp}K_0^{exp}}{V_0^{DFT}K_0^{DFT}}\left[F^{DFT}\left(V\frac{V_0^{DFT}}{V_0^{exp}}\right) - F^{DFT}(V_0^{DFT})\right] + \Delta F(V,T) \quad \text{Equation 2}$$

$V_0^{exp}$ was taken to be 40.6 Å$^3$ (Dobson and Jacobsen, 2004), 65.6 Å$^3$ (Sasaki et al., 1982) and 18.7 Å$^3$ (Tsirelson et al., 1998) for bridgmanite, ringwoodite and periclase respectively whereas $K_0$ was taken to be 256.7 (Tange et al., 2012), 184 (Kojitani et al., 2016) and 160.64 GPa (Tange et al., 2009). $K_0^{DFT}$ was determined statically using a stress-strain method with 4 strains of -0.02, -0.01, 0.01 and 0.02 and was determined to be 231.5, 173.7 and 150.9 GPa respectively. Since the three different phases have slightly different pressure corrections, we corrected the pressures of each individual phase and then recalculated the relationships between the phases. If we consider a "transition pressure" as the pressure at which the chemical potential of ringwoodite is equal to that of bridgmanite plus MgO at a fixed temperature then for Reaction 1 this pressure moves from 22.0 GPa to 22.8 GPa at 1873 K. The effect

of water on the position and Clapeyron slope of the transition is independent of this correction. Both the uncorrected and the corrected pressure values are shown in Figure 1, for all latter figures and tables the uncorrected pressures are shown for simplification. Using an LDA functional produces unphysical transition pressures even when the data is corrected using Equation 1 and 2 above (see Yu et al. (2007) and Figure S3) and so we have not included the LDA predictions here.

*Error Propagation*

QHA calculations do not have an obvious method for determining error. Instead we shall use the error from molecular dynamics calculations which give similar answers to the QHA. This was determined using the blocking method of Flyvbjerg and Petersen (1989) to be <2.5 meV/atom. To propagate this error through to our phase diagrams we used a numerical method. Firstly the bridgmanite, periclase and ringwoodite phase were assigned a random energy selected from a normal distribution centred on their standard energy and with a standard error of 2.5 meV/atom. Secondly, the common tangent or phase boundary was calculated at the pressure and temperature of interest. Third- the first two steps were repeated 1000000 times. Fourth all of our results were fit to a normal distribution and 1σ errors were determined and reported. This process was then repeated at each pressure and temperature of interest.

## 3. Results:

*3.1 Dry Post Spinel Transition:*

Figure 1 and Table 1 shows our DFT calculated transition pressures for dry ringwoodite converting into bridgmanite and MgO:

$Mg_2SiO_4 \rightarrow MgSiO_3 + MgO$ Reaction 1

Our calculated phase transition is roughly in the middle of the experimental range. At 1873 K (the average temperature at 660 km depth) we find that the transition occurs at 22.7 GPa which corresponds to a depth of 614 (594 km). This is somewhat shallower than the average depth of the 660 of 647-654 km (Gu and Dziewonski, 2002), but this discrepancy could be resolved either by the addition of water (see below), a cooler geotherm or by a different pressure correction. Other compositions might also affect the transition pressure, although the addition of iron has been demonstrated to produce only very

small (~0.1 GPa) effects on the phase boundary (Ishii et al., 2019; Ito and Takahashi, 1989). While there is a possibility that Fe and water may have coeffects upon the phase transition, studies of iron-containing ringwoodite have observed no major change in absorption frequency or intensity of OH peaks when compared to iron-free ringwoodite (Bolfan-Casanova et al., 2018; Panero et al., 2013; Thomas et al., 2015). This suggests that iron and water are largely independent in ringwoodite and do not form Fe-water complexes which would lead to strong coeffects.

We find a Clapeyron slope at 1873 K of -3.19±0.19 MPa/K. This slope is similar to some experimental studies (Akaogi et al., 2007; Bina and Helffrich, 1994; Hernandez et al., 2015; Irifune et al., 1998; Shim et al., 2001), as well as two previous theoretical determinations – that of Yu *et al*. (2007) (-2.6 to -2.9 MPa/K) and that of Hernandez *et al.* (2015) (-3.4 MPa/K)**.** Notably, our Clapeyron slope is quite non-linear – a fact previously observed by Hernandez *et al.* (2015) and Bina and Helffrich (1994). Importantly the strong non-linearity of the Clapeyron slope means that its value is sensitive to the temperature at which it is measured, and in fact our Clapeyron slope varies from -1.35 MPa/K at 1000 K to -3.47 MPa/K at 2000 K. This non-linearity at high pressures may be missed in experimental studies with few data points, and assuming a linear phase boundary may result in a significantly underestimated slope. This behaviour may go some way to explaining the different slopes in the literature. Overall, we conclude that the appropriate value of the slope at 1873 K is -3.19±0.19 MPa/K and we agree with the higher Clapeyron slopes found in the literature.

As shown in Table S1 for Reaction 1 the variation of reaction enthalpy ($\Delta H$) with pressure ($d\Delta H/dP$) is not large. On going from 20 to 30 GPa $\Delta H$ of Reaction 1 increases by 0.32 eV/f.u. This is larger than the change in reaction energy induced by temperature ($\Delta S$) across geothermally relevant temperatures but is small enough that both $d\Delta H/dP$ and $d\Delta S/dP$ are important in determining the overall shape of the Clapyeron slope which leads to the non-linear behaviour of the slope.

Another consequence to the small value of $d\Delta H/dP$ is that the error in determining the phase transition is quite large. As seen in Figure 1, even with a quite small error in energy of 2.5 meV/atom the error bars are large. Extremely precise estimates of entropy would be required to reduce this error bar significantly.

223 *3.2 Water Incorporation:*

224 To determine the effect of water on this phase transition we need to consider where water sits
225 in the structures. As outlined in Muir and Brodholt (2018) and Hernandez et al. (2013), in aluminium-
226 free bridgmanite at the conditions of the 660 km discontinuity most water in bridgmanite prefers to fill
227 a Mg vacancy with two $H^+$ atoms and periclase does not take significant amounts of water. Experiments
228 and theoretical work (Fei and Katsura, 2020; Gruninger et al., 2020; Li et al., 2009; Panero, 2010;
229 Panero et al., 2013; Purevjav et al., 2014; Stebbins et al., 2009; Ye et al., 2012) have shown three major
230 incorporation mechanisms for water in ringwoodite - two $H^+$ atoms in a Mg vacancy, four $H^+$ atoms in
231 a Si vacancy, and other complexes that involve Mg exchange with Si. All studies agree that most water
232 is incorporated in the Mg vacancy (when the water concentration is below ~2 wt%), then the Si vacancy
233 and then the more exotic complexes. Water in Mg vacancies typically accounts for around 60-80% of
234 the total absorbed hydrogen (Fei and Katsura, 2020; Gruninger et al., 2020) in ringwoodite. As shown
235 in Table S2 and S3 the introduction of more minor absorption sites for the water in ringwoodite into
236 our calculations has negligible effects on the resultant phase diagram and thus can safely be ignored in
237 our calculations. We therefore only consider the hydrated Mg vacancies in ringwoodite here.

238 The two water bearing phases, ringwoodite and bridgmanite, have quite different vacancy and
239 H geometries. Mg in bridgmanite is 12 coordinated to oxygen whereas it is 6 coordinated in ringwoodite.
240 With each of the two $H^+$ atoms bound to an oxygen there are 66 possible arrangements of hydrogen in
241 bridgmanite and 15 in ringwoodite. The favoured arrangement of hydrogen in bridgmanite is detailed
242 in Muir and Brodholt (2018) and discussed more in the supplementary information section**.** For
243 ringwoodite we find that all arrangements of H are within 6 meV of each other, and moreover, when
244 running a molecular dynamics simulation the hydrogen freely moves between the different oxygens in
245 the vacancy (Figure S2). Thus for both ringwoodite and bridgmanite we shall use the most favoured
246 arrangements of hydrogen to determine the free energy, but at elevated temperatures all arrangements
247 are sampled by MD and considered equally possible for configurational entropy calculations.

248 Using the free energy of each hydrous phase the energy of Reaction 2 can be calculated:

249 $(2H)MgSiO_4 \rightarrow (2H)SiO_3 + MgO$ Reaction 2

The energies of Reaction 2 are listed in Table S1. As outlined in the methods the free energies of Reaction 1 and Reaction 2 are added linearly to achieve the free energy of converting ringwoodite into bridgmanite and periclase with a fixed water concentration (pseudo univariant reaction). As seen in Table 1 the Clapeyron slope for the reaction increases slightly in a wet system under pseudo-univariant conditions, but this is not a thermodynamically favoured system as will be seen below.

The errors induced into the dry phase transition by small $d\Delta H/dP$ differences are even larger in the wet phase transition. While the introduction of water to the system causes large differences in enthalpy (Table S1) which are easily resolved with standard methods, the wet phase diagram relies upon how the free energy of each phase changes with water concentration ($dE/dx$). As an approximation, varying the concentration of water (x) in each system can be considered as taking a system with some amount of water in it and adding units of dry ringwoodite or bridgmanite and periclase. Adding these dry units makes very little change to $dH/dP$ on either side of the phase transition as explained above and thus as x is varied there is little variation in $d\Delta H/dP$ and $dE/dP$. The error in the phase diagram which relies on fitting common tangents of $dE/dx$ is therefore large, as is the error in fitting Clapeyron slopes which rely on the derivative of $dE/dP$. This is somewhat unavoidable due to the similar energetics of each side of the phase transition and will only be eased at very large concentrations of water.

*3.3 Phase Diagrams for water bearing system:*

Using the above results we construct a phase diagram for the post-spinel transition as a function of water. This is shown in Figure 2. It should be noted that this phase diagram does not include a free water phase and so implicitly assumes infinite solubility of water in all phases; the effect of limited solubility of water in ringwoodite is discussed below. Two major effects are noticeable.

First, the addition of water pushes the post-spinel transition to deeper depths, however, the magnitude of this is highly dependent on the water concentration (some values are given in Table S4). At low water concentrations, the transition depth is essentially unaffected by water up to a concentration of about 100 ppm or so. Above that concentration, the phase transition is gradually pushed to higher pressures, and with 2 wt% water at 1873 K the phase transition begins <40 km deeper. The effect is

similar at other temperatures, and at 2000 K the transition depth increases by <48 km with 2% water. With 1 wt% water we find that the transition pressure increases by 0.35 GPa (0.2-0.6 GPa with error) at 1873 K. With 2 wt% water we find that the transition pressure increases by 1.42 GPa (1.16-1.68 with error) at 1873 K. This can be compared to Higo et al. (2001) where ~1 wt% water was observed to shift the transition pressure by ~+0.2 GPa, papers by Litasov *et al.* (Litasov et al., 2005a; Litasov et al., 2005b) where 2 wt% water lead to a change in transition pressure of ~+0.4 GPa and Ghosh et al. (2013) where 2 wt% led to a change in transition pressure of +1-1.3 GPa. Our 1 wt% results are in line with Higo and Litasov, our 2 wt% results are in line with Ghosh. Variations of the water content lead to strong fluctuation of this number with the key parameter being how much water is present in ringwoodite and whether ringwoodite saturation is exceeded.

Second, the transition broadens into a coexistence region of all three phases (a three-phase loop). Again, the effect is highly dependent on the water content, with the width of the loop being essentially zero up to about 100 ppm after which it broadens considerably. These loops become very broad due to the fact that water strongly favours ringwoodite over bridgmanite. However, as mentioned above, these phase diagrams do not consider a free water phase. A plausible phase diagram which considers a free water phase is shown in Figure 3.

To determine the full phase diagram in Figure 3 we need to know the free energy of water. While free energies of water exist in the literature, it is not clear how reliable they are at these P&T conditions. We can avoid this, however, if we simply know the water saturation limit of ringwoodite (or bridgmanite) at the appropriate temperature and pressure. The saturation limit of ringwoodite has been examined previously and is likely to be around 1-2 wt% at the conditions of the 660 km discontinuity (Fei and Katsura, 2020; Inoue et al., 2010; Keppler and Bolfan-Casanova, 2006; Kleppe et al., 2002; Ohtani et al., 2000; Pearson et al., 2014; Smyth et al., 2003). Figure 3 has been constructed by assuming a ringwoodite saturation of 1 wt% (10,000 wt. ppm), the most recent estimate for water solubility at TZ conditions (Fei and Katsura, 2020). This concentration of water in ringwoodite at saturation then determines the top of the two-phase loop via the horizontal line in Figure 3. The intersection of this horizontal line with the left-hand side of the phase loop also determines the solubility of water in bridgmanite. The phase boundary between the bridgmanite + periclase and bridgmanite +

306 periclase + water fields is unconstrained in our system and so we have drawn it as a vertical line. A
307 similar diagram is found in Higo et al. (2001). It should be noted that "free water" will generally not
308 be free at 660 conditions as it will likely form a hydrous silicate melt (see for example (Fei, 2021; Fei
309 and Katsura, 2020)). The general effect of forming a hydrous melt is lowering the saturation level of
310 ringwoodite as the free energy of the hydrous melt is lower than that of silicate+water. However, the
311 ringwoodite saturation of ~1 wt% water chosen in this study was determined in the presence of melt
312 and so the phase diagram is consistent with any excess water being incorporated into a melt.

313 4. Geophysical Implications:

314 *4.1 Transition Width and Water Content*

315 Figure 3 shows the two phase-loop for a maximum water solubility in ringwoodite of 1 wt%.
316 As can be seen, the width of the phase loop is negligible for water contents less than about 1000 ppm,
317 but then grows rapidly to become about 10 km wide, before shrinking again as the water content
318 approaches ringwoodite saturation. The width of the transition is also plotted in Figure 4, alongside the
319 uncertainty. The maximum width depends on the maximum solubility of water in ringwoodite as shown
320 in Figure S4, but the general trend will be the same.

321 The 660 transition is thought to be extremely narrow (<2 km) as it is a strong reflector of 1 Hz
322 seismic waves (Xu et al., 2003). Such a narrow transition is possible in dry Fe-containing ringwoodite
323 (Ishii et al., 2019), but as shown in Figure 3 and 4, water can cause the transition to be very wide. For
324 such a narrow transition to occur the water concentration must be either very low or alternatively near
325 the saturation limit of ringwoodite. To obtain a phase loop with < 2 km width at 1873 K the bottom of
326 the transition zone must have less than about 700 wt. ppm water or alternatively more than about 8500
327 wt. ppm water , assuming ringwoodite saturation of 1 wt%. In the lower water case, the water content
328 is below the solubility of water in bridgmanite and so the transition produces bridgmanite and MgO
329 only, whereas the high water case exceeds the solubility of bridgmanite and a free water phase is also
330 produced. Such a scenario has been previously proposed in a dehydration melting process at the top of
331 the lower mantle (Schmandt et al., 2014). As noted above our chosen saturation concentration of 1%
332 was determined in the presence of melt (Fei and Katsura, 2020) and thus our phase diagram is consistent
333 with the presence of melt above the ringwoodite saturation.

Many studies place transition zone water contents at around a few thousand ppm - at least locally if not globally (Houser, 2016; Huang et al., 2005; Li et al., 2009; Mao et al., 2012; Panero, 2010; Sun et al., 2015; Thio et al., 2016; Ye et al., 2012; Yoshino et al., 2008). This corresponds to the broadest parts of the phase loop and thus it is implied that regions of the 660 km discontinuity with these water contents would be essentially invisible to seismic reflectors. Alternatively, some studies (Fei et al., 2017) place the transition zone water content close to ringwoodite saturation which would be consistent with a very wet ringwoodite phase leading to a narrow phase loop.

It should be noted that our calculated transition widths are thermodynamic maximums and the effective width (as seen by seismic waves) of the real transition loop would be somewhat smaller (Stixrude, 1997. This is because a large proportion of the transition can occur over a small depth range (i.e. consider the lever rule for phase proportions as pressure is increased within the loop). In Figure 4 we show the width of the loop (in km) over which a proportion of ringwoodite is transformed. For instance, for a water content of ~800 ppm, it takes about 7 km to transform all the ringwoodite into bridgmanite plus periclase and so nominally this transition would not be sharp to high frequency seismic waves. 90% of the transition, however, occurs within only the first 2 km, and so actually this transition would be seismically sharp. Similarly at the high water content end; with a water content of 8000 ppm, only 20% of the ringwoodite is transformed over the first ~3 km while the remaining 80% transforms instantaneously (assuming no kinetics) as it hits the univariant line (horizontal line in Figure 3). This too will appear sharp. Quantifying the exact effect is difficult in this system due to the small energy differences between hydrated ringwoodite and bridgmanite and the small amounts of water that go into bridgmanite. Nevertheless, the width of the phase loop increases sharply with increasing water content and thus the narrow width of the 660 km is a strong control on the water content at the bottom of the transition zone and it must be either low or high. This also opens up another way for testing regions suggested to have water contents of between about 1000 to 7000 ppm, since high frequency seismic reflectors should not be observed or should be very weak.

*4.2 Topography of the 660 km discontinuity:*

The 660 transition has observed topographical variations of up to ~40 km (see for example (Andrews and Deuss, 2008; Day and Deuss, 2013; Deuss et al., 2006; Gu and Dziewonski, 2002; Guo and Zhou, 2020; Jenkins et al., 2016). As outlined above a very large amount of water, > 1.5 wt%, would be required to depress the onset of the phase transition by 40 km. For concentrations up to about 1000 ppm, the depression of the transition would be essentially 0 km. Water alone cannot, therefore, be responsible for all the topography on the 660 km discontinuity.

Water is also found to not substantially alter the Clapeyron slope of the transition (Table 2). If we define the Clapeyron slope either by the first appearance of bridgmanite and ferropericlase or by the conversion of 50% ringwoodite then there is little change in the Clapeyron slope up to 1 wt% water. This is important because it means both the dry and the wet transition of ringwoodite have high Clapeyron slopes. We find that the observed variations in transition depth of up to 35 km can be caused by temperature variations of ~500 K in both the dry and wet cases. This means that thermal variation is a plausible explanation for all observed topographical variations in the 660 discontinuity. This suggestion agrees with thermal modelling which concludes that discontinuities in the 660 are thermal in origin because they are positively correlated with wave speed perturbations (Guo and Zhou, 2020). In contrast Wang et al. (2020) conclude that temperature and varying amounts of water are required to explain both the 660 topography and the velocities about the 660 km. The different conclusions may have to do with the particular tomographic model used in the different studies but in either case water alone cannot reproduce these effects. The low Clapeyron slope suggested in some previous studies would rule out a thermal origin for these effects as temperatures would have to fluctuate by thousands of degrees.

*4.3 Maximum Bridgmanite Water Concentration*

If we consider the univariant phase transition following the method of Hernandez *et al.*(2013), we calculate a partition coefficient of 8.5-8.6 at both 1873 and 2000 K. This compares favourably with a previous theoretical value of 10 (Hernandez et al., 2013) obtained from 0 K energies, and experimental values spread between 9-24 (Inoue et al., 2010). Assuming a ringwoodite saturation of 1 wt%, this means that bridgmanite should be able to contain ~1000 ppm water. However, a univariant transition results in an overestimate of the amount of water in bridgmanite, and in principle we can also estimate

bridgmanite saturation by considering the phase loop (Figure 3 and S5). For a ringwoodite saturation of 1 wt%, bridgmanite saturation at 1873 K is about 500 ppm (between 300-800 ppm when considering the uncertainties). Thus transition zone water contents above about 800 ppm are likely to saturate bridgmanite and a downward convecting mantle will produce a free water phase. This estimate is similar to that of Higo et al. (2001) where they found experimentally a similar phase diagram with ~1 wt% water in ringwoodite but ~0.05 wt% water in bridgmanite.

## 5 Conclusions:

In this paper we conclude that:

i) Water has a large effect on the width of the coexistence region (three phase loop) of the post-spinel transition. To satisfy the seismic observations of a narrow 660 discontinuity, the water content at the base of the transition zone must be low (<~700 ppm) or high (>~8000 ppm); intermediate amounts of water would broaden the discontinuity making it invisible to high-frequency seismic waves. Moreover, this may offer a way of confirming regions of the lower TZ that are suspected of having moderate water contents. An important caveat is that the effective width of the transition may be smaller than the maximum width measured here which needs further study.

ii) Water only has a very small effect on the Clapeyron slope of the post-spinel transition and thus the range of depths observed for the 660 km discontinuity cannot be explained just by variations in water. Moreover, our Clapeyron slope is in agreement with high values in the literature and so observed variations in the depth to the 660 km can be explained by temperature variations of ~500 K. We also conclude that the Clapeyron slope is strongly non-linear and so needs to be measured carefully.

iii) Water has a moderate effect on the depth of the post-spinel transition. 1 wt% water increases the depth by about 8 km

## Acknowledgments:

The research in this proposal was supported by National Natural Science Foundation of China (41773057) and by NERC Grants NE/H021027/1 and NE/M00046X/1. JM is highly thankful to Chinese Academy of Sciences (CAS) for PIFI. Calculations were run on the UK National HPC facility, ARCHER. We would like to thank Kei Hirose and an anonymous reviewer for suggesting helpful changes to the manuscript.

418

419 Bibliography

420


421 Akaogi, M., Takayama, H., Kojitani, H., Kawaji, H., Atake, T., 2007. Low-temperature heat capacities,
422 entropies and enthalpies of Mg2SiO4 polymorphs, and alpha-beta-gamma and post-spinel phase
423 relations at high pressure. *Phys. Chem. Minerals* 34, 169-183.
424 Andrews, J., Deuss, A., 2008. Detailed nature of the 660 km region of the mantle from global receiver
425 function data. *J. Geophys. Res.-Sol. Ea.* 113.
426 Bina, C.R., Helffrich, G., 1994. Phase-transition clapeyron slopes and transition zone seismic
427 discontinuity topography. *J. Geophys. Res.-Sol. Ea.* 99, 15853-15860.
428 Bolfan-Casanova, N., Schiavi, F., Novella, D., Bureau, H., Raepsaet, C., Khodja, H., Demouchy, S.,
429 2018. Examination of Water Quantification and Incorporation in Transition Zone Minerals:
430 Wadsleyite, Ringwoodite and Phase D Using ERDA (Elastic Recoil Detection Analysis). *Frontiers in*
431 *Earth Science* 6.
432 Day, E.A., Deuss, A., 2013. Reconciling PP and P'P' precursor observations of a complex 660 km
433 seismic discontinuity. *Geophys. J. Int.* 194, 834-838.
434 Deuss, A., Redfern, S.A.T., Chambers, K., Woodhouse, J.H., 2006. The nature of the 660-kilometer
435 discontinuity in Earth's mantle from global seismic observations of PP precursors. *Science* 311, 198-
436 201.
437 Dobson, D.P., Jacobsen, S.D., 2004. The flux growth of magnesium silicate perovskite single crystals.
438 *Am. Mineral.* 89, 807-811.
439 Fei, H., Yamazaki, D., Sakurai, M., Miyajima, N., Ohfuji, H., Katsura, T., Yamamoto, T., 2017. A nearly
440 water-saturated mantle transition zone inferred from mineral viscosity. *Science Advances* 3.
441 Fei, H.Z., 2021. Water Content of the Dehydration Melting Layer in the Topmost Lower Mantle.
442 *Geophys. Res. Lett.* 48.
443 Fei, H.Z., Katsura, T., 2020. High water solubility of ringwoodite at mantle transition zone
444 temperature. *Earth Planet. Sci. Lett.* 531.
445 Fei, Y., Van Orman, J., Li, J., van Westrenen, W., Sanloup, C., Minarik, W., Hirose, K., Komabayashi, T.,
446 Walter, M., Funakoshi, K., 2004. Experimentally determined postspinel transformation boundary in
447 Mg2SiO4 using MgO as an internal pressure standard and its geophysical implications. *J. Geophys.*
448 *Res.-Sol. Ea.* 109.
449 Flyvbjerg, H., Petersen, H.G., 1989. Error-estimates on averages of correlated data. *J. Chem. Phys.* 91,
450 461-466.
451 Ghosh, S., Ohtani, E., Litasov, K.D., Suzuki, A., Dobson, D., Funakoshi, K., 2013. Effect of water in
452 depleted mantle on post-spinel transition and implication for 660 km seismic discontinuity. *Earth*
453 *Planet. Sci. Lett.* 371, 103-111.
454 Gruninger, H., Liu, Z.D., Brauckmann, J.O., Fei, H.Z., Ballaran, T.B., Martin, T., Siegel, R., Kentgens,
455 A.P.M., Frost, D.J., Senker, J., 2020. Hydroxyl Defects and Oxide Vacancies within Ringwoodite-
456 toward Understanding the Defect Chemistry of Spinel-Type Oxides. *Journal of Physical Chemistry C*
457 124, 12001-12009.
458 Gu, Y.J., Dziewonski, A.M., 2002. Global variability of transition zone thickness. *J. Geophys. Res.-Sol.*
459 *Ea.* 107.
460 Guo, Z., Zhou, Y., 2020. Finite-frequency imaging of the global 410-and 660-km discontinuities using
461 SS precursors. *Geophys. J. Int.* 220, 1978-1994.
462 Hernandez, E., Alfe, D., Brodholt, J., 2013. The incorporation of water into lower-mantle perovskites:
463 A first-principles study. *Earth Planet. Sci. Lett.* 364, 37-43.
464 Hernandez, E.R., Brodholt, J., Alfe, D., 2015. Structural, vibrational and thermodynamic properties of
465 Mg2SiO4 and MgSiO3 minerals from first-principles simulations. *Phys. Earth Planet. Inter.* 240, 1-24.

Higo, Y., Inoue, T., Irifune, T., Yurimoto, H., 2001. Effect of water on the spinel-postspinel transformation in Mg2SiO4. *Geophys. Res. Lett.* 28, 3505-3508.
Houser, C., 2016. Global seismic data reveal little water in the mantle transition zone. *Earth Planet. Sci. Lett.* 448, 94-101.
Huang, X.G., Xu, Y.S., Karato, S.I., 2005. Water content in the transition zone from electrical conductivity of wadsleyite and ringwoodite. *Nature* 434, 746-749.
Inoue, T., Wada, T., Sasaki, R., Yurimoto, H., 2010. Water partitioning in the Earth's mantle. *Phys. Earth Planet. Inter.* 183, 245-251.
Irifune, T., Nishiyama, N., Kuroda, K., Inoue, T., Isshiki, M., Utsumi, W., Funakoshi, K., Urakawa, S., Uchida, T., Katsura, T., Ohtaka, O., 1998. The postspinel phase boundary in Mg2SiO4 determined by in situ x-ray diffraction. *Science* 279, 1698-1700.
Ishii, T., Huang, R., Fei, H., Koemets, I., Liu, Z., Maeda, F., Yuan, L., Wang, L., Druzhbin, D., Yamamoto, T., Bhat, S., Farla, R., Kawazoe, T., Tsujino, N., Kulik, E., Higo, Y., Tange, Y., Katsura, T., 2018. Complete agreement of the post-spinel transition with the 660-km seismic discontinuity. *Scientific Reports* 8.
Ishii, T., Huang, R., Myhill, R., Fei, H.Z., Koemets, I., Liu, Z.D., Maeda, F., Yuan, L., Wang, L., Druzhbin, D., Yamamoto, T., Bhat, S., Farla, R., Kawazoe, T., Tsujino, N., Kulik, E., Higo, Y., Tange, Y., Katsura, T., 2019. Sharp 660-km discontinuity controlled by extremely narrow binary post-spinel transition. *Nat. Geosci.* 12, 869-+.
Ishii, T., Kojitani, H., Akaogi, M., 2011. Post-spinel transitions in pyrolite and Mg2SiO4 and akimotoite-perovskite transition in MgSiO3: Precise comparison by high-pressure high-temperature experiments with multi-sample cell technique. *Earth Planet. Sci. Lett.* 309, 185-197.
Ito, E., Takahashi, E., 1989. Postspinel transformations in the system Mg2SiO4-Fe2SiO4 and some geophysical implications. *Journal of Geophysical Research-Solid Earth and Planets* 94, 10637-10646.
Jenkins, J., Cottaar, S., White, R.S., Deuss, A., 2016. Depressed mantle discontinuities beneath Iceland: Evidence of a garnet controlled 660 km discontinuity? *Earth Planet. Sci. Lett.* 433, 159-168.
Katsura, T., Yamada, H., Shinmei, T., Kubo, A., Ono, S., Kanzaki, M., Yoneda, A., Walter, M.J., Ito, E., Urakawa, S., Funakoshi, K., Utsumi, W., 2003. Post-spinel transition in Mg2SiO4 determined by high P-T in situ X-ray diffractometry. *Phys. Earth Planet. Inter.* 136, 11-24.
Keppler, H., Bolfan-Casanova, N., 2006. Thermodynamics of water solubility and partitioning, in: Keppler, H., Smyth, J.R. (Eds.), Water in Nominally Anhydrous Minerals, pp. 193-230.
Kleppe, A.K., Jephcoat, A.P., Smyth, J.R., 2002. Raman spectroscopic study of hydrous gamma-Mg2SiO4 to 56.5 GPa. *Phys. Chem. Minerals* 29, 473-476.
Kojitani, H., Inoue, T., Akaogi, M., 2016. Precise measurements of enthalpy of postspinel transition in Mg2SiO4 and application to the phase boundary calculation. *J. Geophys. Res.-Sol. Ea.* 121, 729-742.
Kresse, G., Furthmuller, J., 1996. Efficient iterative schemes for *ab-initio* total-energy calculations using a plane-wave basis set. *Phys. Rev. B* 54, 11169-11186.
Kresse, G., Joubert, D., 1999. From ultrasoft pseudopotentials to the projector augmented-wave method. *Phys. Rev. B* 59, 1758.
Li, L., Brodholt, J., Alfe, D., 2009. Structure and elasticity of hydrous ringwoodite: A first principle investigation. *Phys. Earth Planet. Inter.* 177, 103-115.
Litasov, K., Ohtani, E., Sano, A., Suzuki, A., Funakoshi, K., 2005a. In situ X-ray diffraction study of post-spinel transformation in a peridotite mantle: Implication for the 660-km discontinuity. *Earth Planet. Sci. Lett.* 238, 311-328.
Litasov, K.D., Ohtani, E., Sano, A., Suzuki, A., Funakoshi, K., 2005b. Wet subduction versus cold subduction. *Geophys. Res. Lett.* 32.
Mao, Z., Lin, J.-F., Jacobsen, S.D., Duffy, T.S., Chang, Y.-Y., Smyth, J.R., Frost, D.J., Hauri, E.H., Prakapenka, V.B., 2012. Sound velocities of hydrous ringwoodite to 16 GPa and 673 K. *Earth Planet. Sci. Lett.* 331, 112-119.
Muir, J.M.R., Brodholt, J.P., 2018. Water distribution in the lower mantle: Implications for hydrolytic weakening. *Earth Planet. Sci. Lett.* 484, 363-369.

Nose, S., 1984. A molecular-dynamics method for simulations in the canonical ensemble. *Mol. Phys.* 52, 255-268.
Ohtani, E., Mizobata, H., Yurimoto, H., 2000. Stability of dense hydrous magnesium silicate phases in the systems Mg2SiO4-H2O and MgSiO3-H2O at pressures up to 27 GPa. *Phys. Chem. Minerals* 27, 533-544.
Panero, W.R., 2010. First principles determination of the structure and elasticity of hydrous ringwoodite. *J. Geophys. Res.-Sol. Ea.* 115.
Panero, W.R., Smyth, J.R., Pigott, J.S., Liu, Z., Frost, D.J., 2013. Hydrous ringwoodite to 5 K and 35 GPa: Multiple hydrogen bonding sites resolved with FTIR spectroscopy. *Am. Mineral.* 98, 637-642.
Pearson, D.C., Brenker, F.E., Nestola, F., Mcneill, J., Nasdala, J., Nasdala, L., Hutchison, M., Matveev, S., Mather, K., Silversmit, G., Schmitz, S., Vekemans, B., Vincze, L., 2014. Hydrous mantle transition zone indicated by ringwoodite included within diamond. *Nature* 507, 221-224.
Perdew, J.P., Ruzsinszky, A., Csonka, G.I., Vydrov, O.A., Scuseria, G.E., Constantin, L.A., Zhou, X.L., Burke, K., 2008. Restoring the density-gradient expansion for exchange in solids and surfaces. *Phys. Rev. Lett.* 100, 1364061-1364064.
Purevjav, N., Okuchi, T., Tomioka, N., Abe, J., Harjo, S., 2014. Hydrogen site analysis of hydrous ringwoodite in mantle transition zone by pulsed neutron diffraction. *Geophys. Res. Lett.* 41, 6718-6724.
Sasaki, S., Prewitt, C.T., Sato, Y., Ito, E., 1982. Single-crystal x-ray study of gamma-Mg2SiO4. *J. Geophys. Res.* 87, 7829-7832.
Schmandt, B., Jacobsen, S., Becker, T., Liu, Z., Dueker, K., 2014. Dehydration melting at the top of the lower mantle. *Science* 344, 1265-1268.
Shim, S.H., Duffy, T.S., Shen, G.Y., 2001. The post-spinel transformation in Mg2SiO4 and its relation to the 660-km seismic discontinuity. *Nature* 411, 571-574.
Smyth, J.R., Holl, C.M., Frost, D.J., Jacobsen, S.D., Langenhorst, F., McCammon, C.A., 2003. Structural systematics of hydrous ringwoodite and water in Earth's interior. *Am. Mineral.* 88, 1402-1407.
Stebbins, J.F., Smyth, J.R., Panero, W.R., Frost, D.J., 2009. Forsterite, hydrous and anhydrous wadsleyite and ringwoodite (Mg2SiO4): Si-29 NMR results for chemical shift anisotropy, spin-lattice relaxation, and mechanism of hydration. *Am. Mineral.* 94, 905-915.
Sun, W., Yoshino, T., Sakamoto, N., Yurimoto, H., 2015. Hydrogen self-diffusivity in single crystal ringwoodite: Implications for water content and distribution in the mantle transition zone. *Geophys. Res. Lett.* 42, 6582-6589.
Tange, Y., Kuwayama, Y., Irifune, T., Funakoshi, K.-i., Ohishi, Y., 2012. P-V-T equation of state of MgSiO3 perovskite based on the MgO pressure scale: A comprehensive reference for mineralogy of the lower mantle. *J. Geophys. Res.-Sol. Ea.* 117.
Tange, Y., Nishihara, Y., Tsuchiya, T., 2009. Unified analyses for P-V-T equation of state of MgO: A solution for pressure-scale problems in high P-T experiments. *J. Geophys. Res.-Sol. Ea.* 114.
Thio, V., Cobden, L., Trampert, J., 2016. Seismic signature of a hydrous mantle transition zone. *Phys. Earth Planet. Inter.* 250, 46-63.
Thomas, S.M., Jacobsen, S.D., Bina, C.R., Reichert, P., Moser, M., Hauri, E.H., Koch-Muller, M., Smyth, J.R., Dolinger, G., 2015. Quantification of water in hydrous ringwoodite. *Frontiers in Earth Science* 2.
Togo, A.T., I., 2015. First principles phonon calculations in materials science. *Scripta Materialia* 108, 1-5.
Tsirelson, V.G., Avilov, A.S., Abramov, Y.A., Belokoneva, E.L., Kitaneh, R., Feil, D., 1998. X-ray and electron diffraction study of MgO. *Acta Crystallographica Section B-Structural Science* 54, 8-17.
Wang, X., Chen, Q.F., Niu, F.L., Wei, S.J., Ning, J.Y., Li, J., Wang, W.J., Buchen, J., Liu, L.J., 2020. Distinct slab interfaces imaged within the mantle transition zone. *Nat. Geosci.*
Xu, F., Vidale, J.E., Earle, P.S., 2003. Survey of precursors to P ' P ': Fine structure of mantle discontinuities. *J. Geophys. Res.-Sol. Ea.* 108.

566 Ye, Y., Brown, D.A., Smyth, J.R., Panero, W.R., Jacobsen, S.D., Chang, Y.-Y., Townsend, J.P., Thomas,
567 S.-M., Hauri, E.H., Dera, P., Frost, D.J., 2012. Compressibility and thermal expansion of hydrous
568 ringwoodite with 2.5(3) wt% H2O. *Am. Mineral.* 97, 573-582.
569 Yoshino, T., Manthilake, G., Matsuzaki, T., Katsura, T., 2008. Dry mantle transition zone inferred from
570 the conductivity of wadsleyite and ringwoodite. *Nature* 451, 326-329.
571 Yu, Y.G., Wentzcovitch, R.M., Tsuchiya, T., Umemoto, K., Weidner, D.J., 2007. First principles
572 investigation of the postspinel transition in Mg2SiO4. *Geophys. Res. Lett.* 34.

573

574

Figure Captions:

Figure 1: Phase boundaries for the post-spinel transition (ringwoodite to bridgmanite and periclase) under water free conditions from our *ab initio* results here (black dashed line) compared to phase boundaries from the literature (solid lines are experimental results, dotted lines are theoretical). We show our results with no pressure correction (lower pressure line) as well as with the GGA pressure correction (higher pressure line). The grey shading represents the calculated error on our pressure corrected value. I89= Ito 1989 I98=Irifune 1998, S01=Shim 2001 K04=Katsura 2004 F04= Fei 2003 L05= Litasov 2005 Y07= Yu 2007 A08=Akaogi 2008 I11= Ishi 2011 G13=Ghosh 2013 H13= Hernandez 2013 K16= Kojitani 2016 I18= Ishii 2018a

Figure 2: Phase diagram of the post-spinel transition as a function of water concentration (wt. ppm) at three temperatures (blue=1550, black=1873 and red=2000 K). The error bounds (as outlined in the methods) for 1873 K are presented as shaded regions whereas those of 2000 and 1500 K are presented as dotted lines. Some values of this transition are listed in Table S4 for clarity.

Figure 3: Plot of the 1873 K phase diagram with ringwoodite saturation set to 1 wt% (10,000 ppm). The error bars have been excluded for clarity but are shown in Figure 2 and in Figure 4. The line separating the bdg+MgO and the bdg+MgO+Water regions is not calculated here and so has been set vertical. The numbers next to the vertical yellow, red and green lines indicate (i) the change in depth of the onset of the transition relative to the dry transition, and (ii) the width of the transition, at three water concentrations (530, 2000 and 9000 ppm). The yellow line represents the maximum width of the phase transition loop.

Figure 4: This shows the width of the phase loop as a function of water content (see Figure 3) at 1873 K for a saturation of ringwoodite of 10,000 ppm (1 wt%) (solid black line). In **A** the uncertainty is shown as dotted lines and the red line indicates the concentration of water at a transition width of of 2 km. The water concentrations (in wt. ppm) are also given in red. The same graph at 2000 K is shown in Figure S5. **B** shows the width of the transition over which different percentages of the ringwoodite undergoes the transition (dotted lines). For instance, if the amount water is 700 ppm, 90% of ringwoodite has converted to bridgmanite and MgO over just 1 km, while the other 10% transforms over a further 6 km. This would effectively lead to a sharp transition.

Table 1: The transition pressure (the pressure at which the chemical potential of ringwoodite is equal to that of bridgmanite and MgO at a fixed temperature) for dry and wet (10,000 ppm) ringwoodite at different temperatures determined by the four different methods outlined in the methods. The slope of the transition was determined via a second order polynomial fit to these points. The crossover for wet bridgmanite is the pseudo-univariant system where mixed phases are not allowed to form. This is not a thermodynamically favoured system but allows easy comparison of the different energy methods.

Table 2 Clapeyron Slopes (in MPa/K) at 1873 K determined as in Table 1 for dry and wet systems. In the wet system the Clapeyron slope was defined either as the first onset of bdg+MgO or when 50% of the ringwoodite has converted. Ringwoodite saturation was set to 1 wt%. In the wet systems the slope error increases hugely as it is a derivative of a curve that is rapidly changing at 1873 K and the wet system has large errors (see Figure 2) but the pressure values at each temperature are similar in the wet and dry cases (see Table S4).

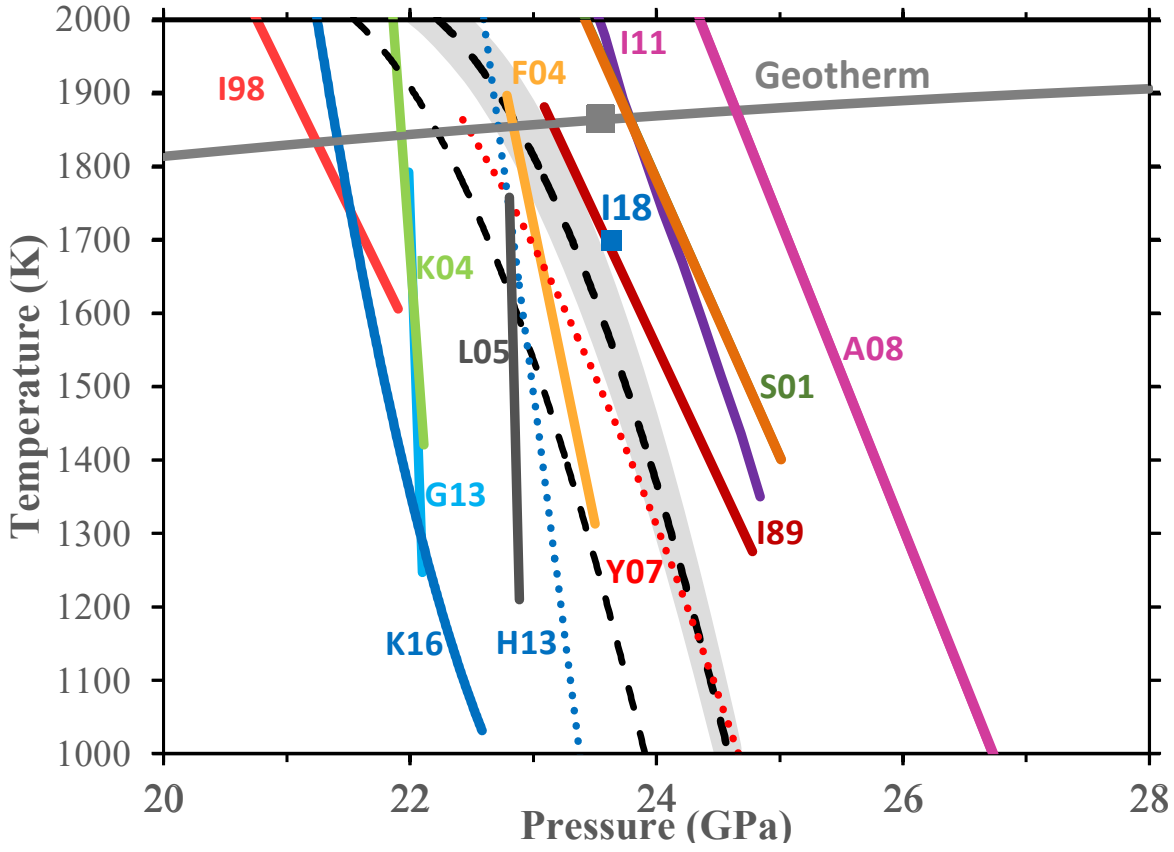
2000
1900
1800
1700
1600
1500
1400
1300
1200
1100
1000
Temperature (K)
20
22
24
26
28
Pressure (GPa)
I98
F04
I11
Geotherm
I18
K04
L05
A08
S01
G13
I89
Y07
K16
H13

Figure 1

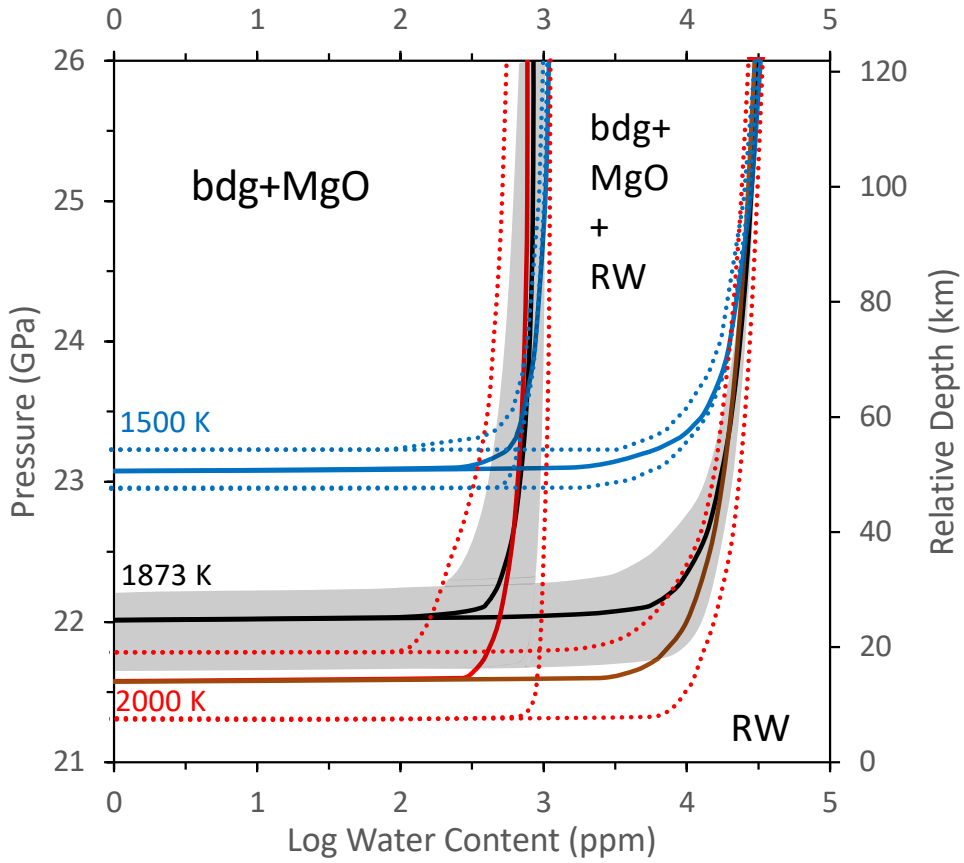
bdg+MgO
bdg+
MgO
+
RW
1500 K
1873 K
2000 K
RW
Pressure (GPa)
Relative Depth (km)
Log Water Content (ppm)
0
1
2
3
4
5
21
22
23
24
25
26
0
20
40
60
80
100
120

Figure 2

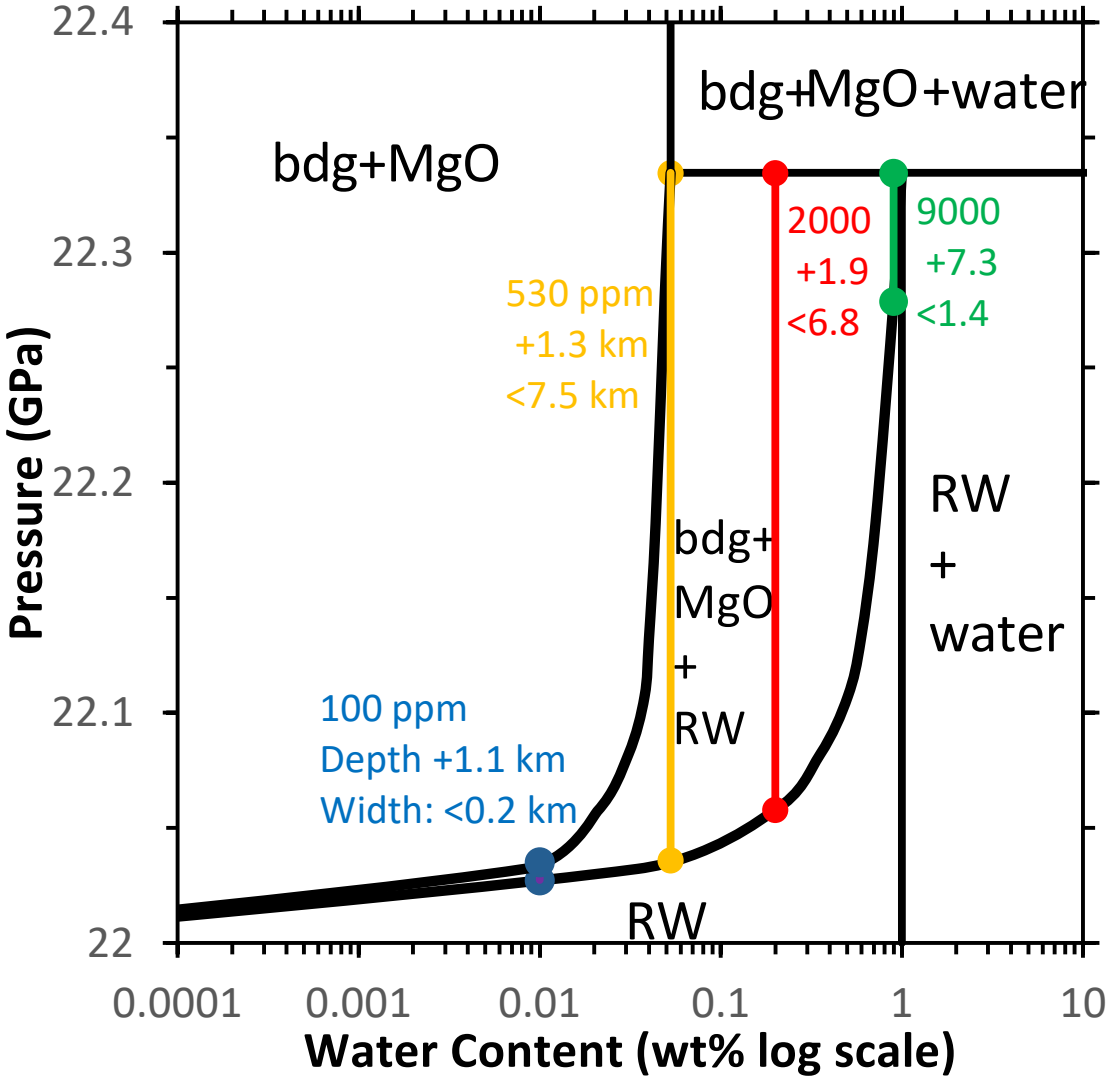


660

661 Figure 3

662

663

664

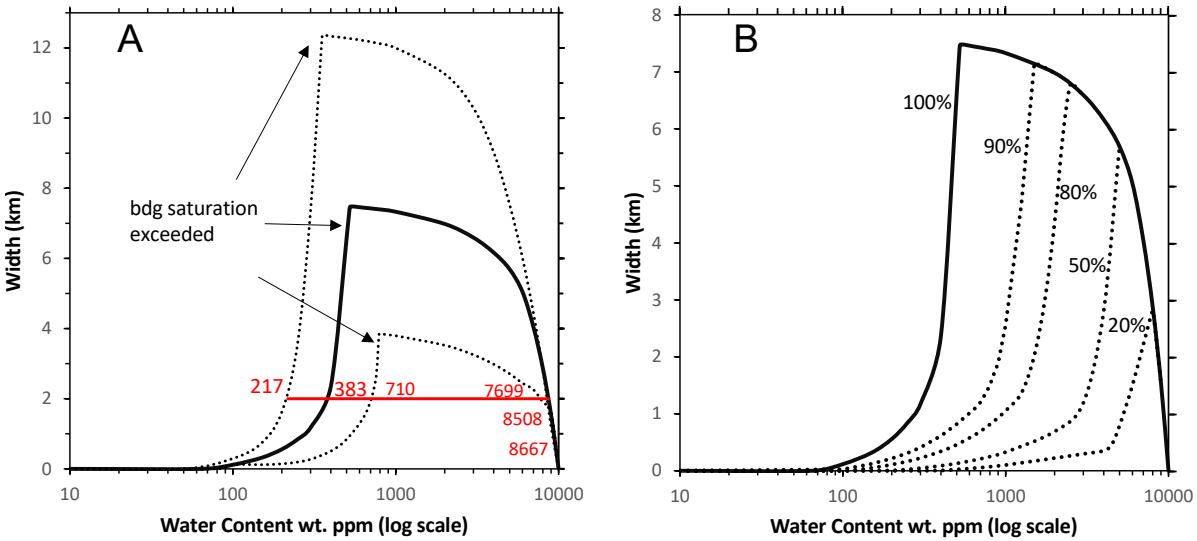


665

666 Figure 4

667

668

| | | 0 | 1000 | 1500 | 2000 | Slope at 1873 K (MPA/K) |
|---|---|---|---|---|---|---|
| Dry | ENTH | 24.18 | 23.83 | 22.91 | 21.46 | -3.14 |
| | MD | 24.18 | 23.83 | 22.91 | 21.40 | -3.22 |
| | QHA | 24.18 | 23.84 | 22.89 | 21.38 | -3.26 |
| | TI | 24.18 | 23.91 | 23.08 | 21.54 | -3.19 |
| Wet | ENTH | 24.97 | 24.39 | 23.73 | 21.70 | -3.68 |
| | MD | 24.97 | 24.41 | 23.67 | 21.49 | -4.01 |
| | QHA | 24.97 | 24.41 | 23.69 | 21.50 | -4.01 |
| | TI | 24.97 | 24.41 | 23.67 | 21.45 | -4.07 |

Table 1: The transition pressure (the pressure at which the chemical potential of ringwoodite is equal to that of bridgmanite and MgO at a fixed temperature) for dry and wet (10,000 ppm) ringwoodite at different temperatures determined by the four different methods outlined in the methods. The slope of the transition was determined via a second order polynomial fit to these points. The crossover for wet bridgmanite is the pseudo-univariant system where mixed phases are not allowed to form. This is not a thermodynamically favoured system but allows easy comparison of the different energy methods.

| | Dry | Water= 1000 wt. ppm | 10000 wt. ppm |
|---|---|---|---|
| Onset | -3.19±0.19 | -3.16±0.47 | -3.16±0.76 |
| 50% converted | -3.19±0.19 | -3.19±0.56 | -3.16±0.81 |

Table 2 Clapeyron Slopes (in MPa/K) at 1873 K determined as in Table 1 for dry and wet systems. In the wet system the Clapeyron slope was defined either as the first onset of bdg+MgO or when 50% of the ringwoodite has converted. Ringwoodite saturation was set to 1 wt%. In the wet systems the slope error increases hugely as it is a derivative of a curve that is rapidly changing at 1873 K and the wet system has large errors (see Figure 2) but the pressure values at each temperature are similar in the wet and dry cases (see Table S4).